Biology of Reproduction, 2017, 96(1), 232–243
doi:10.1095/biolreprod.116.144451
Research Article
Advance Access Publication Date: 23 December 2016

Research Article

Acidification of uterine epithelium during embryo implantation in mice†

Shuo Xiao[1,2,‡], Rong Li[1,2,‡], Ahmed E. El Zowalaty[1,2], Honglu Diao[1,3], Fei Zhao[1,2], Yongwon Choi[4] and Xiaoqin Ye[1,2,*]

[1]Department of Physiology and Pharmacology, College of Veterinary Medicine, University of Georgia, Athens, Georgia, USA; [2]Interdisciplinary Toxicology Program, University of Georgia, Athens, Georgia, USA; [3]Reproductive Medical Center, Renmin Hospital, Hubei University of Medicine, Shiyan, Hubei, China and [4]Department of Pathology and Laboratory Medicine, University of Pennsylvania School of Medicine, Philadelphia, Pennsylvania, USA

*Correspondence: Department of Physiology and Pharmacology, College of Veterinary Medicine, Interdisciplinary Toxicology Program, University of Georgia, 501 DW Brooks Dr., Athens, GA 30602, USA. Tel: +1-706-542-6745; Fax: +1-706-542-3015; E-mail: ye@uga.edu

†**Grant Support:** This work was supported by the National Institutes of Health (NIH R15HD066301 and NIH R01HD065939 to XY).

Conference presentation: Presented in part at the:
- University of Georgia Interdisciplinary Toxicology Program Annual Retreat, April 13, 2012, Athens, Georgia,
- 45th Annual Meeting of the Society for the Study of Reproduction, August 12–15, 2012, State College, Pennsylvania,
- Southeastern Society of Toxicology Annual Meeting, October 8–9, 2012, Athens, Georgia,
- University of Georgia Interdisciplinary Toxicology Program Annual Retreat, April 5, 2013, Athens, Georgia,
- Frontiers in Reproduction Symposium, June 7–9, 2013, Woods Hole, Massachusetts,
- 46th Annual Meeting of the Society for Study of Reproduction, July 22–26, 2013, Montreal, Canada,
- Gordon Research Conference (Mammalian Reproduction), August 10–15, 2014, New London, New Hampshire.

‡These authors contributed equally to the work.

Received 21 August 2016; Revised 23 October 2016; Accepted 22 November 2016

Abstract

Uterine luminal epithelium (LE) is essential for establishing uterine receptivity. Previous microarray analysis revealed upregulation of *Atp6v0d2* in gestation day 4.5 (D4.5) LE in mice. Realtime PCR showed upregulation of uterine *Atp6v0d2* starting right before embryo attachment ~D4.0. In situ hybridization demonstrated specific uterine localization of *Atp6v0d2* in LE upon embryo implantation. *Atp6v0d2* encodes one subunit for vacuolar-type H^+-ATPase (V-ATPase), which regulates acidity of intracellular organelles and extracellular environment. LysoSensor Green DND-189 detected acidic signals in LE and glandular epithelium upon embryo implantation, correlating with *Atp6v0d2* upregulation in early pregnant uterus. *Atp6v0d2*$^{-/-}$ females had significantly reduced implantation rate and marginally reduced delivery rate from first mating only, but comparable number of implantation sites and litter size compared to control and comparable fertility to control from subsequent matings, suggesting a nonessential role of Atp6v0d2 subunit in embryo implantation. Successful implantation in both control and *Atp6v0d2*$^{-/-}$ females was associated with uterine epithelial acidification. No significant compensatory upregulation of *Atp6v0d1* mRNA was detected in D4.5 *Atp6v0d2*$^{-/-}$ uteri. To determine the role of V-ATPase instead of a single subunit in embryo implantation, a specific V-ATPase inhibitor bafilomycin A1 (2.5 μg/kg) was injected via uterine fat pad on D3 18:00 h. This treatment resulted in reduced uterine epithelial acidification,

delayed implantation, and reduced number of implantation sites. It also suppressed oil-induced artificial decidualization. These data demonstrate uterine epithelial acidification as a novel phenomenon during embryo implantation and V-ATPase is involved in uterine epithelial acidification and uterine preparation for embryo implantation.

Summary Sentence

Our findings that mouse uterine epithelium becomes more acidic upon embryo implantation initiation and suppression of uterine epithelial acidification adversely affects embryo implantation provide a novel direction for understanding mechanisms in establishing uterine receptivity.

Key words: embryo implantation, uterine epithelial acidification, *Atp6v0d2*, V-ATPase, bafilomycin A1, uterine fat pad injection.

Introduction

A receptive uterus is indispensable for the success of embryo implantation, which is a mandatory step for the success of mammalian reproduction. Precise cellular and molecular mechanisms of how a uterus transforms into a receptive state is far from being well understood [1–3]. Uterine epithelium includes luminal epithelium (LE) that lines up the uterine lumen and glandular epithelium (GE) that extends from LE into the underlying stromal layer. Luminal epithelium is the first layer of cells that an embryo communicates with for embryo implantation and is also essential for uterine receptive sensitivity [4, 5]. Glandular epithelium secretes molecules critical for embryo development and uterine preparation for embryo implantation [6]. Embryo implantation is associated with dynamic morphological and molecular changes in the LE [7–9]. It is expected that the dynamic expression of certain genes in the peri-implantation LE will hold a key to understanding mechanisms for the establishment of uterine receptivity. Our microarray analysis reveals Atpase, H^+ transporting, lysosomal V0 subunit D2 (*Atp6v0d2*) as one of the most highly expressed and most highly upregulated genes in the gestation day 4.5 (D4.5) LE compared to the preimplantation D3.5 LE [4].

Atp6v0d2 encodes the more tissue-specific d subunit of the vacuolar-type H^+-ATPase (V-ATPase). The d2 subunit is potentially involved in assembling the integral V0 domain and the peripheral V1 domain of V-ATPase [10]. The transmembrane integral V0 domain is composed of six subunits (a, c, c′, c″, d, and e) and involved in proton translocation, while the cytoplasmic peripheral V1 domain contains eight subunits (A–H) and is responsible for ATP hydrolysis [11–13]. The ATP-dependent proton transport by V-ATPase is from the cytoplasmic compartment to the opposite side of the membrane, which can be either the lumen of intracellular organelles (e.g., lysosomes, endosomes, and secretory vesicles) or the lumen of extracellular environment (e.g., epididymal lumen), to acidify the intracellular organelles or the extracellular environment, respectively [11]. Besides different cellular localizations, different tissue distributions and different utilizations of specific subunit(s) may also contribute to the diverse functions of V-ATPase [14, 15].

V-ATPase is crucial for male reproduction [16, 17]. Most of the V-ATPase subunits are strongly expressed in the apical side of rodent epididymal and vas deferens epithelium to establish and maintain an acidic luminal environment for sperm maturation and storage [18]. The importance of this acidic luminal environment has also been demonstrated in *c-ros* and forkhead box i1 (*Foxi1*) deficient male mice, which lack several V-ATPase subunits leading to increased epididymal luminal pH and infertility, with the latter caused by the defective movement of spermatozoa through the female reproductive tract for fertilization [19, 20].

The potential roles of V-ATPase in female reproduction, especially uterine epithelial function during embryo implantation, are largely unknown. One study demonstrates that three V-ATPase subunits (A, B, and c) are highly expressed in bovine uterine LE at the beginning of embryo–maternal interaction, suggesting potential participation of the uterine V-ATPase in embryo implantation [21]. A histochemical study finds increased lysosomal numbers and activity in D5.5 (postimplantation initiation) rat uterine epithelium compared to that in the nonpregnant state (estrus or diestrus stages) [22]. Lysosome is the most acidic organelle in the cell, and V-ATPase is a key regulator of lysosomal pH [23]. The upregulation of a V-ATPase subunit *Atp6v0d2* in D4.5 LE [4] would suggest a potential function of V-ATPase in LE acidification and uterine preparation for embryo implantation. It was therefore hypothesized that *Atp6v0d2* upregulation was important for LE acidification, and LE acidification was critical for embryo implantation. This hypothesis was tested using both genetic approach (*Atp6v0d2*$^{-/-}$ females) and pharmacological approach (V-ATPase inhibitor bafilomycin A1) in mice.

Materials and methods

Reagents

TRIzol, Superscript III and 20 × Saline-Sodium Citrate, LysoSensor Green DND-189 (Invitrogen, Carlsbad, CA, USA); dNTPs (Biomiga, San Diego, CA, USA); Taq DNA polymerase (Lucigen, Middleton, WI, USA); power SYBR Green PCR master and 384-well plates (Applied Biosystems, Carlsbad, CA, USA); superfrost plus slides, triton X-100 and formamide (Fisher Scientific, Pittsburgh, PA, USA); bafilomycin A1 and sesame oil (Sigma, St. Louis, MO, USA); Evans blue dye (Alfa Aesar, Ward Hill, MA, USA); isoflurane (Webster Veterinary, Devens, MA, USA); pGEM-T vector (Promega, Madison, WI, USA); DIG RNA labeling mix, blocking reagent, antidigoxigenin antibody, and NBT/BCIP (Roche Diagnostics, Indianapolis, IN, USA); methyl green, levamisole hydrochloride, and dextran sulfate sodium salt (MP biomedicals, Solon, OH, USA); iScript Reverse Transcription Supermix for RT-qPCR, SsoAdvanced Universal SYBR Green Supermix (Bio-rad, Hercules, CA, USA); primers for realtime PCR (Integrated DNA Technologies, Coralville, IA, USA).

Animals

C57BL6/129 mixed background wild type (WT), *Atp6v0d2*$^{+/-}$, and *Atp6v0d2*$^{-/-}$ mice were derived from Dr. Yongwon Choi's colony

at University of Pennsylvania and genotyped as previously described [24]. C57BL6/129 mixed background WT mice that were not used as a control for *Atp6v0d2*$^{-/-}$ mice were derived from our *Lpar3* mouse colony [25, 26]. Mice were housed in polypropylene cages with free access to regular food and water from water sip tubes in a reverse osmosis system. The animal facility is on a 12-h light/dark cycle (6:00 AM to 6:00 PM) at 23 ± 1°C with 30–50% relative humidity. All methods used in this study were approved by the University of Georgia IACUC Committee (Institutional Animal Care and Use Committee) and conform to National Institutes of Health guidelines and public law.

Luminal epithelium isolation and uterine tissue collection

Young virgin WT females or *Atp6v0d2*$^{-/-}$ females were mated naturally with WT stud males and checked for a vaginal plug the next morning. The day a vaginal plug identified was designated as gestation day 0.5 (D0.5, mating night as D0). D3.5 and D4.5 LE cells were isolated as previously described using 0.5% dispase and gentle scraping [4, 27]. Uterine tissues were collected from euthanized WT females between 11:00 h and 12:00 h on D0.5, D2.5, D3.5, D4.5, and D5.5, and midnight of D4.0. Uterine tissues from *Atp6v0d2*$^{-/-}$ females and their littermates were collected between 11:00 h and 12:00 h on D3.5 and D4.5. Both uterine horns from D0.5 and D2.5 females were quickly removed and snap-frozen on dry ice. Oviducts from these mice were flushed with 1 × PBS for the presence of embryos/oocytes to determine the pregnancy status. About one-third of a uterine horn from each euthanized D3.5 female was frozen on dry ice for tissue sectioning. The remaining D3.5 uterine horns were flushed with 1 × PBS (to determine the status of pregnancy and to remove embryos for uterine gene expression study) and frozen on dry ice for realtime PCR. On D4.5 and D5.5, mice were anesthetized with isoflurane by inhalation and intravenously (i.v.) injected with Evans blue dye to visualize the implantation sites as previously described [28]. Uterine horns from D4.5 and D5.5 were frozen on dry ice for RNA isolation and/or tissue sectioning. In addition, flushed uterine horns from pseudopregnant and pregnant mice on D3.5 at 22:00 h were also collected and frozen. At least three pregnant mice were included in each group.

RNA isolation and realtime PCR

For quantitative gene expression in WT females, total RNAs from LE and uterus were isolated using TRIzol, and cDNA was prepared using Superscript III reverse transcriptase with random primers. Realtime PCR was performed in 384-well plates using SYBR Green I intercalating dye on ABI 7900. For quantitative gene expression between *Atp6v0d2*$^{-/-}$ and WT females, total RNA from D3.5 and D4.5 uteri and D4.5 LE was isolated using TRIzol, and cDNA was prepared using iSript Reverse Transcription Supermix for Realtime PCR, which was performed in 384-well plates using SsoAdvanced Universal SYBR Green Supermix on CFX384 Real-Time System. Primer sequences were listed in Table 1. The mRNA expression levels of *Atp6v0a1*, *Atp6v0a2*, *Atp6v0a3*, *Atp6v0a4*, *Atp6v0b*, *Atp6v0c*, *Atp6v0d1*, *Atp6v0d2*, *Atp6v0e1*, *Atp6v0e2*, mucolipin-1 (*Mcoln1*), two pore segment channel 1 (*Tpcn1*), chloride channel, voltage sensitive 7 (*Clcn7*), cystic fibrosis transmembrane conductance regulator (*Cftr*), hypoxanthine phosphoribosyltransferase 1 (*Hprt1*), and glyceraldehyde 3-phosphate dehydrogenase (*Gapdh*) were determined by realtime PCR. Two housekeeping genes, *Gapdh* and *Hprt1*, were used as controls.

Table 1. Gene-specific primer sequences used in realtime PCR and/or in situ hybridization.

Gene	Primer sequence	PCR product size (bp)
Atp6v0a1	F: AGGCAGCTGCTAAGAACA R: AAAATCTCCGAACATCACAG	395
Atp6v0a2	F: CATCTACCACATGCTCAACA R: AGTCTGGGGTGATTCTCATT	388
Atp6v0a3	F: GCTACTGCTGGAGACCTTG R: CTGTTCTCCAAGGTGGATG	380
Atp6v0a4	F: AAACAGAGTCTCACCGACAG R: CCAACCTGTTCTGTGGAGT	391
Atp6v0b	F: TACACAGTCACCATCAGCAG R: GAAGGGGAAGGTGATGATAG	383
Atp6v0c	F: TGGTGGTGGCAGTACTTATC R: GCACTAGGACACTGCACATT	398
Atp6v0d1	F: TGAAGCTGC ACCTACAGAGT R: TTCATCTCATCAAGGTCCTG	390
Atp6v0d2	F: GAGATGGAAGCTGTCAACAT R: TCTGCCACTCTCTTCATCTG	398
Atp6v0e1	F: GGACCACAGTTGAAAAATGA R: GTCTCGCAGCAATTCTTAAA	384
Atp6v0e2	F: CACCCATCTGTATGACCATC R: TATTTCAACACGGTGGAGAC	390
Mcoln1	F: CCTCTTCATCTACATGGTGC R: CTTGGATCAGTTCACCAGC	241
Tpcn1	F: ATGCCTCTGATGGAACAGG R: ACCTTCCTGGAGGTAGATTG	368
Clcn7	F: CATGGCCAACGTCTCTAAG R: GGTTGATTCGTCTTTCCTCC	341
Cftr	F: CGAGCCAAAAGCATTGACC R: GTGGATAAGCTGGGGATTCT	307
Hprt1	F: GCTGACCTGCTGGATTACAT R: CAATCAAGACATTCTTTCCAGT	172
Gapdh	F: GCCGAGAATGGGAAGCTTGTCAT R: GTGGTTCACACCCATCACAAACAT	205
Abp1	F: TACCCTAATGGTGTGATGGA R: TCAGCCATAGAGTGGATCTG	398

F: forward primer; R: reverse primer, 5′→3′.

In situ hybridization

In situ hybridization was done as previously described [4, 29–31]. The primer sequences used for making sense and antisense probes were listed in Table 1.

LysoSensor Green DND-189 staining

LysoSensor Green DND-189 is an acidotropic fluorescence probe that becomes fluorescent only when it is inside acidic compartments (pKa ∼ 5.2) and its fluorescence intensity correlates with intracellular acidity thus serves as an intracellular pH indicator [32–35]. To investigate uterine epithelial acidification during estrous cycle (determined by vaginal smear [36–38]), early pregnancy, and artificial decidualization [39] in WT mice, as well as in D4.5 *Atp6v0d2*$^{-/-}$ females with or without detectable implantation sites, 2 μl of LysoSensor Green DND-189 (2 μM) was injected into both uterine horns ∼20 min before dissection ∼11:00–12:00 h. Uterine horns were frozen on dry ice. Frozen uterine sections were heated at 55°C for 20 min and detected for fluorescence under a fluorescent microscope with excitation at 488 nm and emission at 505 nm. At least three mice were examined at each time point except for estrous cycle, in which two mice each at proestrus, estrus, metestrus, and diestrus were examined. At least two sections from each uterus were evaluated; for

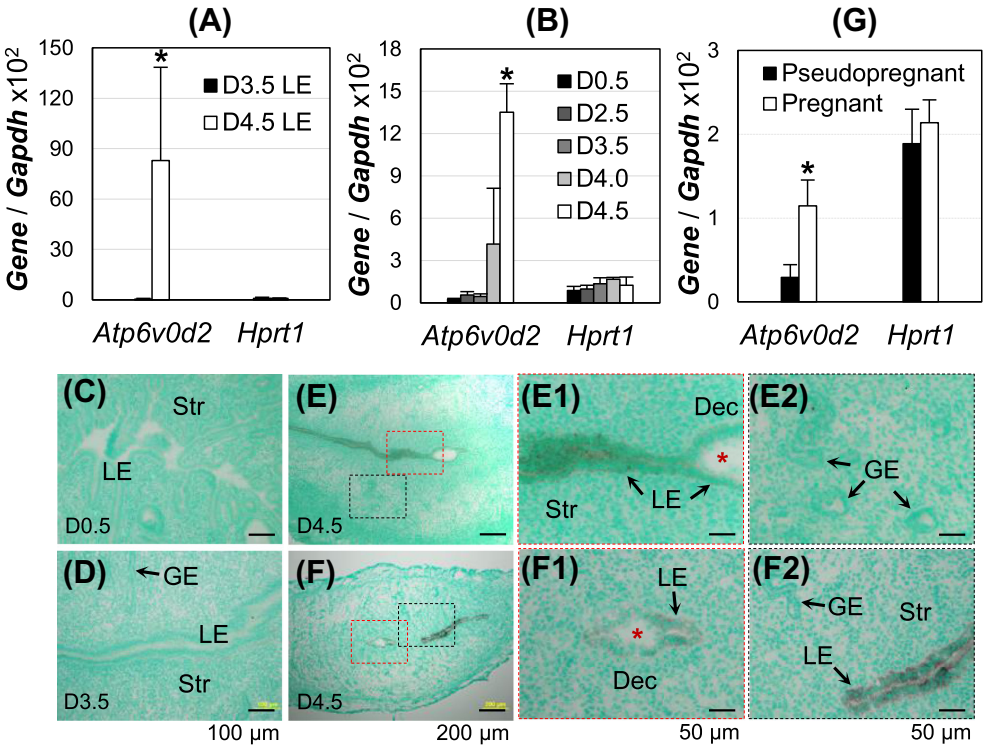

Figure 1. Spatiotemporal expression of *Atp6v0d2* in early pregnant WT mouse uterus. (A, B, G) Realtime PCR, normalized with *Gapdh* and *Hprt1* as a second control; $^*P < 0.05$; error bar: standard deviation; (C–F) in situ hybridization, counterstained with methyl green; D4.0, gestation day 4.0, about time for embryo attachment in mice. (A) *Atp6v0d2* mRNA expression in D3.5 and D4.5 LE, N = 5–6. (B) *Atp6v0d2* mRNA expression level in peri-implantation uterus, N = 4–6. (C–F) Localization of *Atp6v0d2* mRNA in D0.5 (C), D3.5 (D), and D4.5 (E, F) uteri. E1 and E2, enlarged images from the red and black rectangle areas in E, respectively; F1 and F2, enlarged images from the red and black rectangle areas in F, respectively; red *, embryo; LE, uterine luminal epithelium; GE, uterine glandular epithelium; Str, stroma; Dec, decidual zone; scale bar, 100 μm (C, D), 200 μm (E, F), or 50 μm (E1, E2, F1, F2). (G) *Atp6v0d2* mRNA expression in pseudopregnant and pregnant uterus at D3 22:00 h. N = 4–5.

those with implantation sites, at least one implantation site per female and two sections per implantation site were evaluated.

Fertility test in *Atp6v0d2*$^{-/-}$ females

Young virgin (2 months old) *Atp6v0d2*$^{-/-}$ females (N = 19) and their littermate control females (N = 18, *Atp6v0d2*$^{+/+}$ or *Atp6v0d2*$^{+/-}$) were cohabitated with the same stud males. Copulation plug was checked every morning. Cohabitation continued till late pregnancy. Some females had multiple plugs before a term pregnancy occurred. All the females delivered their first litters within 3 to 6 weeks from the first day of cohabitation. Gestation period and litter size were recorded.

Embryo implantation in *Atp6v0d2*$^{-/-}$ females

Another set of 2-month-old virgin *Atp6v0d2*$^{-/-}$ females (N = 27) and control females (N = 8, *Atp6v0d2*$^{+/+}$ or *Atp6v0d2*$^{+/-}$, littermates to some of the *Atp6v0d2*$^{-/-}$ females) were mated similarly as for fertility test. Embryo implantation was detected on D4.5 as previously described [28]. The reproductive tracts of eight *Atp6v0d2*$^{-/-}$ females without implantation sites were flushed with 1 × PBS to check the presence of embryos/oocytes. One ovary was fixed for histology.

Uterine fat pad injection

This method was established in rats by Dr. Koji Yoshinaga [40–45] and was adapted in mice by our group to deliver drugs into the uterus without disturbing the intrauterine environment [39]. Young virgin WT females were mated naturally with WT stud males. Plugged females were randomly distributed into control group and V-ATPase inhibitor bafilomycin A1-treated groups. Bafilomycin A1 specifically inhibits V-ATPase via binding to V0 domain [46]. On D3 at 18:00 h, a small incision was made in the dorsolateral region on the right side of flank under anesthesia with isoflurane inhalation. Five microliter vehicle (20% of ethanol in 1× PBS with blue dye to monitor the injection) or bafilomycin A1 (0.5 or 2.5 μg/kg in vehicle) was injected at 1–2 spots on the adipose tissue next to the right uterine horn only. Implantation sites were detected using blue dye injection [28] on D4.5, D5.5, and D7.5 for vehicle control and 2.5 μg/kg bafilomycin A1 treatment groups, and on D4.5 for 0.5 μg/kg bafilomycin A1 treatment group. If no implantation sites on D4.5 were detected, the uterine horns were flushed with 1× PBS to determine the presence and health status of blastocysts. Uterine tissues were snap-frozen and kept in –80°C for in situ hybridization and some were also processed for LysoSensor Green DND-189 staining as described above.

Artificial decidualization

Artificial decidualization was induced as previously described [47]. Briefly, sesame oil (20 μl) was infused intraluminally in the right uterine horn of pseudopregnant WT females on D3.5 at 10:00 h (mating night with vasectomized male mice was defined as D0). On pseudopregnant D3 at 18:00 h, 5 μl of vehicle or bafilomycin A1 (2.5 μg/kg) was injected into the uterine fat pad surrounding the arteries of the oil-infused uterine horn (right side) following the

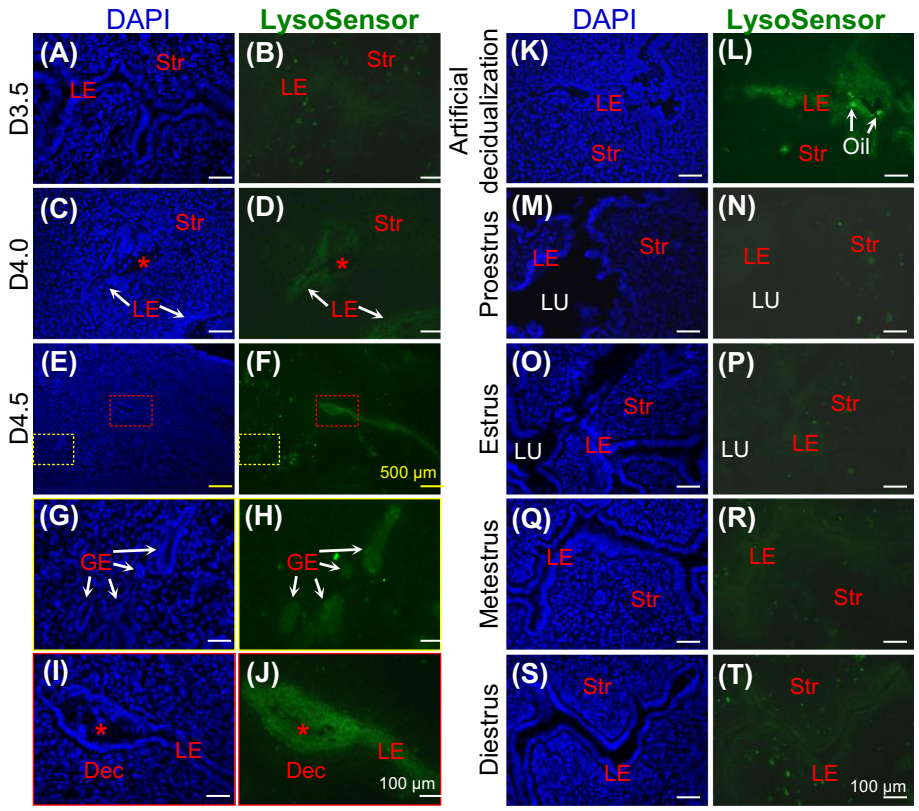

Figure 2. Uterine epithelial acidification during embryo implantation, artificial decidualization, and estrous cycle in WT mice. D4.0, gestation day 4.0, embryo attachment; DAPI, staining nuclei; LysoSensor Green DND-189, reflecting intracellular acidity; LE, uterine luminal epithelium; GE, uterine glandular epithelium; Str, stroma; Dec, decidual zone; LU, uterine lumen; red *, embryo; cross sections (10 μm) of frozen uteri; scale bars, 100 μm (A–D, G–T), or 500 μm (E, F); left panel, DAPI staining of nuclei; right panel, LysoSensor Green DND-189 staining of uterine sections in left panel. (A, B) D3.5 uterus. (C, D) D4.0 uterus. (E, F) D4.5 uterus. (G, H) Enlarged from the yellow rectangles in E and F, respectively. (I, J) Enlarged from the red rectangles in E and F, respectively. (K, L) D4.5 uterus from oil-infused artificial decidualization. Bright green dots in the lumen area were infused oil droplets. (M–T) Different stages of estrous cycle.

procedure described above. On pseudopregnant D7.5, the females were i.v. injected with Evans blue dye to visualize decidual response similar as to visualize implantation sites [28], and the weights of the infused (right) uterine horns were recorded. The right uterine horns were frozen for in situ hybridization to detect a molecular marker *Abp1* for decidual response [48].

Statistical analyses

Two-tail unequal variance Student t-test was used to compare the mRNA expression levels, the numbers of implantation sites, and the weights of the right uterine horns. Two-tailed Fisher exact test was used to compare the rates (e.g., implantation rate and delivery rate). The significant level was set at $P < 0.05$.

Results

Spatiotemporal expression of *Atp6v0d2* in early pregnant wild-type uterus

Our previous microarray analysis revealed upregulation of *Atp6v0a4*, *Atp6v0c*, and *Atp6v0d2*, and downregulation of *Atp6v0a1* and *Atp6v0d1* among all 23 V-ATPase subunits (*Atp6v0a1*, *Atp6v0a2*, *Atp6v0a3*, *Atp6v0a4*, *Atp6v0b*, *Atp6v0c*, *Atp6v0d1*, *Atp6v0d2*, *Atp6v0e1*, *Atp6v0e2*, *Atp6v1A*, *Atp6v1B1*, *Atp6v1B2*, *Atp6v1C1*, *Atp6v1C2*, *Atp6v1D*, *Atp6v1E1*, *Atp6v1E2*, *Atp6v1F*, *Atp6v1G1*, *Atp6v1G2*, *Atp6v1G3*, *Atp6v1H*) in gestation day 4.5 (D4.5) LE compared to D3.5 LE. The differential expression of these genes was modest (<2 fold) except for *Atp6v0d2* [4], which was dramatically upregulated in D4.5 LE. Realtime PCR of isolated LE from D3.5 (preimplantation) and D4.5 (postimplantation initiation) pregnant mice confirmed the dramatic upregulation (>100 fold) of *Atp6v0d2* in D4.5 LE compared to D3.5 LE (Figure 1A). Realtime PCR of early pregnant uteri demonstrated basal levels of expression in preimplantation uteri by D3.5; >8 fold increase in D4.0 uterus compared to D3.5 uterus and continued increase at D4.5 (Figure 1B). In situ hybridization verified the upregulation and LE-specific localization of *Atp6v0d2* upon embryo implantation. *Atp6v0d2* level was lower in the LE at the implantation site compared to nonimplantation site on D4.5 (Figure 1E–F2). No significant expression level of *Atp6v0d2* mRNA was detected in other uterine compartments (Figure 1E2 and F2). *Atp6v0d2* remained highly expressed in the LE on D5.5 (data not shown). The upregulation of *Atp6v0d2* was related to pregnancy since a significantly higher level of *Atp6v0d2* was detected in the pregnant uterus than in the pseudopregnant uterus on D3 at 22:00 h (Figure 1G), right before embryo attachment in pregnant uterus on ~D4.0 [49]. These results demonstrated that *Atp6v0d2* expression in LE was correlated with pregnancy and its upregulation started before implantation initiation and continued during initial stages of embryo implantation.

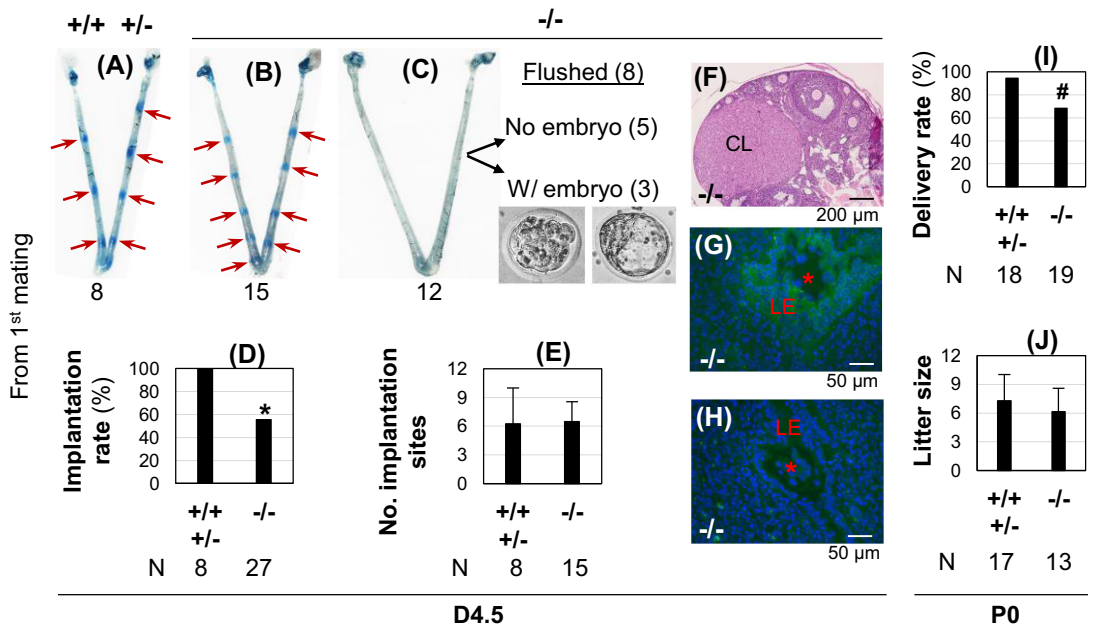

Figure 3. Embryo implantation and fertility in *Atp6v0d2*$^{-/-}$ females from the first mating. +/+ / +/–, WT and heterozygotes as control; –/–, *Atp6v0d2*$^{-/-}$; control females and *Atp6v0d2*$^{-/-}$ females were mated with the same stud males; 8, 15, etc., numbers of mice in each condition/group; red arrow, implantation site; A–H, data from gestation day 4.5 (D4.5); I–J, data from postnatal day 0 (P0). (A) D4.5 control uterus. (B) D4.5 *Atp6v0d2*$^{-/-}$ uterus with implantation sites. (C) D4.5 *Atp6v0d2*$^{-/-}$ uterus without an implantation site. Among the 12 uteri without an implantation site, 8 were flushed, 5 of them with no embryos flushed and remaining 3 with embryos flushed. All the flushed embryos had zona pellucida. (D) D4.5 implantation rate, expressed as the number of mice with implantation site/total number of plugged mice × 100. $^{*}P < 0.05$. (E) Number of implantation sites from the uteri with implantation sites on D4.5. (F) Histology of an ovary from an *Atp6v0d2*$^{-/-}$ mouse without embryo or implantation site as seen in Figure 3C. CL, corpus luteum; scale bar, 200 μm. (G, H) Merged images of DAPI staining (blue) and LysoSensor Green DND-189 staining (green) in uteri with (G) or without (H) detectable implantation sites. LE, uterine luminal epithelium; *, embryo; uterine cross sections (10 μm); scale bar, 50 μm. (I) Delivery rate, expressed as the number of mice delivered pups/total number of plugged mice × 100. #$P = 0.0897$ (two-tailed Fisher exact test). (J) Litter size at birth. (E, J) Error bar, standard deviation.

Uterine epithelial acidification upon implantation initiation

Atp6v0d2 encodes a tissue-specific d subunit of V-ATPase that regulates the acidity of extracellular lumen pH and pH of intracellular organelles [50]. LysoSensor Green DND-189 was used to detect intracellular acidity because it becomes fluorescent only when it is inside acidic compartments (pKa ~ 5.2) [32]. This fluorescent dye detected basal levels of fluorescence in preimplantation pregnant D0.5 and D2.5 uteri (data not shown), basal level fluorescence (data not shown), or above basal level fluorescence in the D3.5 uterine epithelium (Figure 2A and B); detectable signals in D4.0 uterine epithelium (Figure 2C and D); stronger signals in D4.5 uterine epithelium, including LE at both implantation site and interimplantation site and GE (Figure 2E–J); as well as in the D5.5 remaining uterine epithelium but not in the D5.5 implantation chamber where the LE surrounding the embryo had disappeared (data not shown). Strong fluorescence was also detected in the pseudopregnant D4.5 uterine horns with artificial decidualization induced by intrauterine oil infusion (Figure 2K and L) but not in the contralateral uterine horns without oil infusion (data not shown). Fluorescence at basal levels was detected in the nonpregnant uteri at different estrus stages, although the fluorescence in the uterine epithelium at metestrus and diestrus appeared to be above the basal level (Figure 2M–T). LysoSensor Green DND-189 staining did not appear to label the uterine stroma and myometrium during early pregnancy (Figure 2 and data not shown). These data demonstrated increased uterine epithelial acidification during early stages of embryo implantation in mice.

Embryo implantation and fertility in *Atp6v0d2*$^{-/-}$ females

Since upregulation of *Atp6v0d2* correlated with increased uterine epithelial acidification (Figures 1 and 2), did Atp6v0d2 subunit play a role in embryo implantation? *Atp6v0d2*$^{-/-}$ females (2 months old) from first mating had significantly reduced implantation rate compared to their littermate control females (Figure 3A–D). The 15 *Atp6v0d2*$^{-/-}$ mice with detectable implantation sites had a comparable number of implantation sites to the control (Figure 3E). Among the 12 *Atp6v0d2*$^{-/-}$ females without implantation sites, the reproductive tracts of 8 females were flushed, 3 with embryos and 5 without embryos (Figure 3C). Interestingly, all the flushed embryos had intact zona pellucida (Figure 3C), which is normally present in D3.5 embryos but not D4.5 embryos [28, 51, 52]. In addition, all five *Atp6v0d2*$^{-/-}$ females without implantation sites or embryos had corpora lutea (Figure 3F), suggesting ovulation had occurred. LysoSensor Green DND-189 detected uterine epithelial acidification in the *Atp6v0d2*$^{-/-}$ uteri with implantation sites indicated by blue dye reaction (Figure 3G) but not in those without detectable implantation sites, even with the presence of an embryo (Figure 3H). Fertility test indicated marginally reduced ($P = 0.0897$, two-tailed Fisher exact test) delivery rate from the first mating in *Atp6v0d2*$^{-/-}$ females compared to that from the littermate control (Figure 3I). However, the litter size from those delivered *Atp6v0d2*$^{-/-}$ females was not significantly different from the litter size in the control group (Figure 3J). The *Atp6v0d2*$^{-/-}$ females that did not get pregnant from the first mating eventually

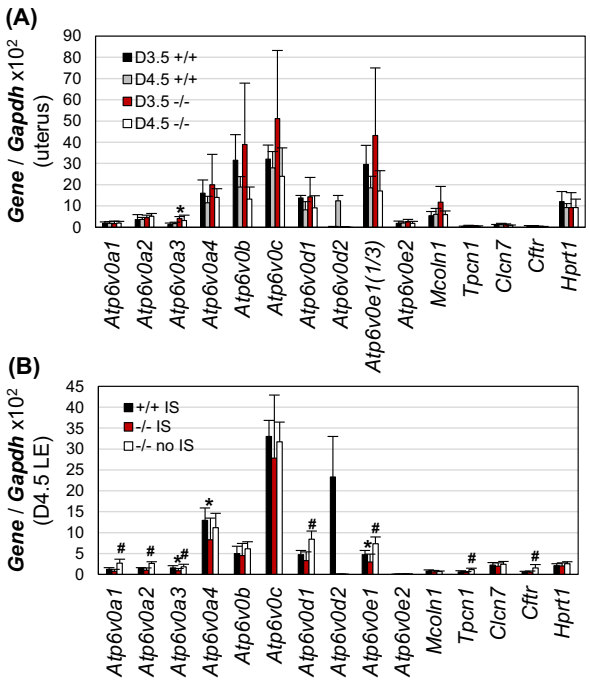

Figure 4. Realtime PCR detecting mRNA levels of V-ATPase V0 subunits and counter ion channels in *Atp6v0d2*$^{-/-}$ uterine LE and uterus. +/+, wild type; –/–, *Atp6v0d2*$^{-/-}$; IS, implantation site; error bar, standard deviation; N = 6–8. (A) mRNA levels of V0 subunits and counter ion channels in D3.5 and D4.5 WT and *Atp6v0d2*$^{-/-}$ uteri with implantation sites. *Atp6v0e1* was shown one-third of its value; $^{*}P < 0.05$, compared to D3.5 +/+. (B) mRNA levels of V0 subunits and counter ion channels in D4.5 WT LE (+/+ IS) and *Atp6v0d2*$^{-/-}$ LE (–/– IS) with implantation sites and D4.5 *Atp6v0d2*$^{-/-}$ LE without implantation sites (–/– no IS). $^{*}P < 0.05$, compared to +/+ IS; $^{\#}P < 0.05$, compared to –/– IS.

became pregnant from the subsequent matings and delivered pups within 6 weeks after cohabitation. They had comparable gestation periods and produced comparable litter sizes as the control (data not shown). These data demonstrate that *Atp6v0d2*-deficiency affected embryo implantation and fertility in some mice from the first mating only and did not affect the overall fertility, and that uterine epithelial acidification was always associated with successful embryo implantation.

Gene expression in *Atp6v0d2*$^{-/-}$ uterus and luminal epithelium

Since *Atp6v0d2* encodes only one of the 14 subunits for a functional V-ATPase, it was possible that there were compensatory regulations, especially of *Atp6v0d1* that also encodes a d subunit, for the loss of *Atp6v0d2* in the uterus and/or LE during embryo implantation. Since the difference in mRNA levels was only observed in some V0 subunits but not any of the V1 subunits between D3.5 LE and D4.5 LE from microarray [4], all the V0 subunits, together with several lysosomal counter ion channels, were examined using realtime PCR. There were no significant changes in mRNA levels between D3.5 WT and D3.5 *Atp6v0d2*$^{-/-}$ uteri except an upregulation of *Atp6v0a3* in the D3.5 *Atp6v0d2*$^{-/-}$ uteri; no significant difference in mRNA levels was detected between D4.5 WT and D4.5 *Atp6v0d2*$^{-/-}$ uteri with implantation sites (Figure 4A). Since *Atp6v0d2* was mainly detected in the LE and potential changes in LE could be obscured in the whole uterus, D4.5 LE was isolated from WT uteri with implantation sites (+/+ IS), *Atp6v0d2*$^{-/-}$ uteri with implantation sites (–/– IS) or without implantation sites (–/– no IS). No significant difference except <1 fold reduction of *Atp6v0a3*, *Atp6v0a4*, and *Atp6v0e1* in the +/+ IS compared to –/– IS was observed (Figure 4B). Several genes, *Atp6v0a1*, *Atp6v0a2*, *Atp6v0a3*, *Atp6v0d1*, *Atp6v0e1*, *Tpcn1*, and *Cftr*, had <3 fold increased expression in the –/– no IS compared to –/– IS (Figure 4B), which might be related to the implantation status because some of these genes, such as *Atp6v0a1*, *Atp6v0d1*, and *Cftr*, showed reduced mRNA levels in D4.5 LE compared to preimplantation D3.5 LE in the microarray analysis [4]. These data indicated no obvious compensatory regulation of related genes at the transcriptional level but did not exclude potential compensatory regulation at other levels than transcription.

Effect of V-ATPase inhibitor bafilomycin A1 on embryo implantation

Since Atp6v0d2 is only one of many subunits for a functional V-ATPase, the nonessential role of *Atp6v0d2* in embryo implantation and female fertility (Figure 3) could not rule out potential function of V-ATPase in uterine epithelial acidification and embryo implantation. Local uterine fat pad injection of 0.5 or 2.5 μg/kg bafilomycin A1 dose-dependently suppressed embryo implantation detected on D4.5 (Figure 5A–C). A uterus from 0.5 μg/kg bafilomycin A1-injected group had four implantation sites on the uninjected side and one implantation site on the injected side (Figure 5B). The sections from the injected side (Figure 5B, red rectangle) had dim green fluorescence in the LE surrounding an embryo without blue dye reaction (Figure 5E, E1), at interimplantation site (Figure 5F, F1), or surrounding an embryo with clear blue dye reaction (Figure 5G, G1), an indication of embryo implantation. The green fluorescence in the LE (Figure 5D, D1) from the uninjected side (Figure 5B, gray rectangle) was stronger than that from the bafilomycin A1-injected site (Figure 5E–G1). Bafilomycin A1 had a similar effect on the green fluorescence intensity in the GE (data not shown) as that in LE. The green fluorescence in the D4.5 uterine epithelium was further lower to barely detectable from mice treated with 2.5 μg/kg bafilomycin A1, especially those without detectable implantation sites (data not shown). These data indicated the inhibitory effect of bafilomycin A1 on uterine epithelial acidification.

The effect of bafilomycin A1 on embryo implantation was confirmed by uterine expression of decidualization marker *Abp1* [48], which was detected in the primary decidual zone of an implantation site in a vehicle-injected uterus (Figure 5A and H), but not in the stromal area of an implantation site in a 2.5 μg/kg bafilomycin A1-treated uterus (Figure 5C and I). The numbers of implantation sites were also determined on D5.5 and D7.5 in vehicle and 2.5 μg/kg bafilomycin A1-treated groups. Bafilomycin A1 treatment significantly reduced the numbers of implantation sites at all three time points compared to vehicle control (Figure 5J). No significant difference in the numbers of implantation sites was observed between D5.5 and D7.5 in the 2.5 μg/kg bafilomycin A1-treated group, but at these two time points, the numbers of implantation sites were significantly higher than that at D4.5 (Figure 5J) and the implantation sites in the D4.5 2.5 μg/kg bafilomycin A1-treated group were faint (Figure 5C), indicating delayed implantation. These data revealed that uterine local fat pad administration of V-ATPase inhibitor bafilomycin A1 not only suppressed uterine epithelial acidification, but also delayed

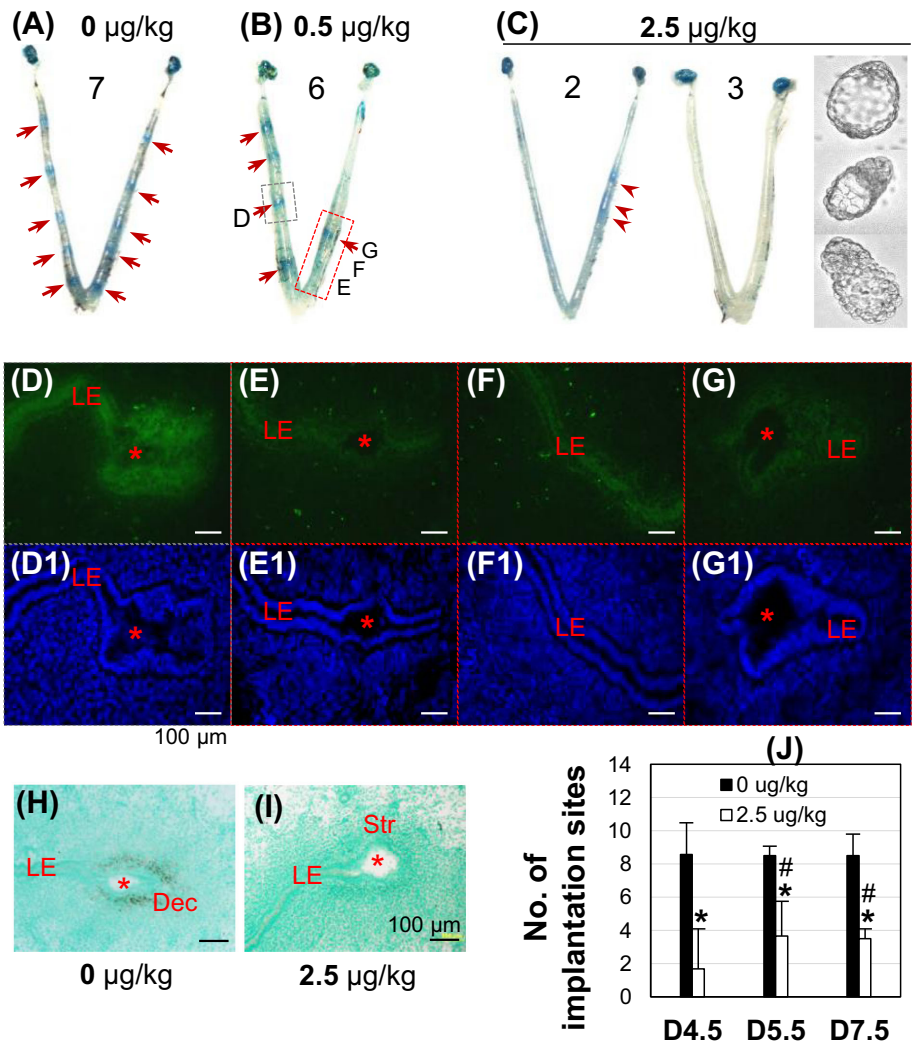

Figure 5. Effects of V-ATPase inhibitor bafilomycin A1 on embryo implantation and uterine epithelial acidification in WT mice. (A–C) Representative uterine images from 0 (A), 0.5 (B), and 2.5 μg/kg (C) bafilomycin A1-treated groups detected on D4.5. Red arrow, defined implantation site; red arrowhead, delayed implantation site; 7, 6, 2, 3, numbers of mice in each condition/group. Embryos in C flushed from the uterine horns without implantation sites. Bafilomycin A1 was injected into uterine fat pad on the right uterine horn on D3 at 18:00 h, 4–6 h before implantation initiation [49]. (D–G) LysoSensor Green DND-189 staining of the implantation site indicated by the gray rectangle (D) and the approximate uterine segments in the red rectangle (no blue dye reaction in the uterine segments for E and F and a clear implantation site for G) in B. (D1–G1) DAPI staining of the sections in D–G, respectively. (H, I) In situ hybridization of decidualization marker *Abp1* in an implantation site from A (H) and a faint implantation site in C (I). (D–I) Red star, embryo; LE, uterine luminal epithelium; Str, stroma; Dec, decidual zone; scale bar, 100 μm. (J) Number of implantation sites in vehicle and 2.5 μg/kg bafilomycin A1-treated groups detected on D4.5, D5.5, and D7.5. Error bar, standard deviation; $^*P < 0.05$, compared to vehicle-treated group; #$P < 0.05$ compared to bafilomycin A1-treated group on D4.5; N = 3–7.

implantation for some embryos, and prevented implantation for other embryos.

Effect of V-ATPase inhibitor bafilomycin A1 on decidualization

To eliminate any potential effect of bafilomycin A1 on embryos in implantation (Figure 5) and to further demonstrate the effect of bafilomycin A1 on uterine function during embryo implantation, uterine fat pad injection of 2.5 μg/kg bafilomycin A1 was performed in an oil-induced artificial decidualization mouse model. Suppression of artificial decidualization upon bafilomycin A1 treatment was indicated by significant reduction of the right (treated side) uterine horn weight on D7.5 in the treated group compared to that in the control group (Figure 6A–D and H), as well as reduced expression of a uterine decidualization marker *Abp1* [48] in the treated group (Figure 6F and G) compared to that in the control group (Figure 6E).

Discussion

This study demonstrates a novel phenomenon that uterine epithelium becomes more acidic during the initial stages of embryo implantation. Increased uterine epithelial acidity is readily detectable at the time of embryo attachment ~D4.0 in natural pregnant uterus and in artificially decidualized pseudopregnant D4.5 uterus by LysoSensor Green DND-189 dye, indicating that uterine epithelial acidification is associated with early uterine preparation for embryo implantation in the presence of an embryo or other stimulus, such as oil, in the uterus.

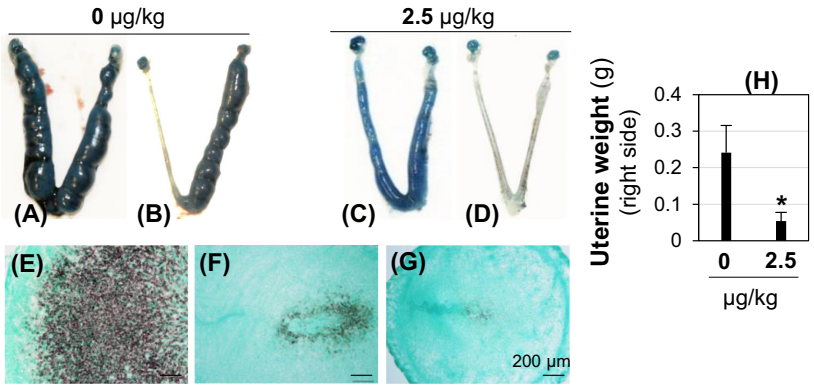

Figure 6. Effect of bafilomycin A1 on artificial decidualization detected on pseudopregnant D7.5 WT mice. Artificial decidualization was induced by intraluminal oil injection on right side and bafilomycin A1 treatment was also on the right side via uterine fat pad injection. (A–D) Representative uteri from vehicle (A, B) or bafilomycin A1 injection (C, D). A and C shows decidualization on both uterine horns due to oil leakage from the right side. (E–G) Detection of decidualization marker *Abp1* on right uterine horns by in situ hybridization. E from B; F from C; G from D; Scale bar, 200 μm. (H) Weight of right uterine horn (injected side). Error bar, standard deviation; N = 4; $^*P < 0.05$.

Although no report is available in the literature about uterine epithelial acidification upon embryo implantation in any species, the following studies imply that uterine epithelial acidification might be a common phenomenon. Striking increases in enzymatic activity of acid phosphatase, which is stored in the lysosome and requires optimal acidic pH, were observed in the uterine LE during initial stages of embryo implantation in rat, mouse, and rabbit [53]. Increased lysosomal numbers and activity were found in D5.5 rat uterine epithelium (postimplantation initiation) compared to nonpregnant state (estrus or diestrus stages) [22]. Transmission electron microscopic study of bovine endometrium detected lysosomes and autolysosomes in the LE at the initial stages of embryo implantation [54]. Three V-ATPase subunits were highly expressed in the bovine LE during early stages of embryo implantation and became pericellularly localized, instead of the apical localization seen in the nonpregnant LE [21]. Although no human uterine epithelial data are available, microarray data (identifier GSE6364) of human endometrium at proliferative and secretory phases in normal and endometriosis patients revealed significant upregulation of several highly expressed V-ATPase subunits in the secretory (receptive) phase but such upregulation was abolished in the endometrium of endometriosis patients [55]. The underlying mechanisms for uterine epithelial acidification upon embryo implantation have never been investigated.

LysoSensor Green DND-189 becomes fluorescent only when it is inside acidic compartments (pKa ~ 5.2) [32]. Since the lysosome is the most acidic intracellular organelle with pH < 5 [50, 56], uterine epithelial acidification detected by LysoSensor Green DND-189 most likely indicates lysosomal acidification, although acidification of other intracellular organelles could not be ruled out. Lysosome acidity is mainly maintained by ATP-driven proton pump V-ATPase coupled with additional ion transporters to dissipate the transmembrane voltage built up by V-ATPase [57].

V-ATPase is a complex enzyme composed of multiple subunits [14]. Some subunits have multiple isoforms, e.g., a subunit has four isoforms (a1, a2, a3, and a4) identified and d subunit has two isoforms (d1 and d2) identified [58, 59]. Despite amino acid sequence similarity, different V-ATPase subunits can have differential expression patterns. For example, a1 is ubiquitously expressed [59]; a2 is highly expressed in the lung, kidney, and spleen [60]; a3 is mainly detectable in osteoclasts [15]; and a4 is expressed in the kidney and male reproductive tract [18, 58]; d1 is ubiquitously expressed [14], whereas d2 is more dominant in kidney, lung, and osteoclast [61]. The expression patterns of the V-ATPase subunits in the peri-implantation uterus had not been previously investigated. Our previous microarray analysis [4] and this study demonstrated the most dramatic upregulation of *Atp6v0d2* mRNA, moderate differential mRNA expression of some other V0 subunits, and no change of mRNA levels of V1 subunits in the uterine LE upon embryo implantation, indicating the differential expression and regulation patterns of V-ATPase subunits in the uterine LE.

Although the precise functions of each V-ATPase subunit are not fully understood, the differential expression patterns of V-ATPase subunits would suggest potentially different functions of the subunits. Indeed, limited data have demonstrated that mutations in *ATP6V1B1* cause distal renal tubular acidosis in patients [62], mutations in *ATP6V0A4* are associated with atypical progressive sensorineural hearing loss and distal renal tubular acidosis [59, 63], while *Atp6v0d2*-deficiency in mice results in impaired osteoclast fusion and increased bone formation [24]. Although *Atp6v0d2* mRNA was highly upregulated in the LE upon embryo implantation, *Atp6v0d2*$^{-/-}$ females had reduced implantation rate only from the first mating and they had comparable overall fertility as age-matched control, indicating that *Atp6v0d2* was not essential for embryo implantation or female fertility. V-ATPase, together with other ion channels, such as cystic fibrosis transmembrane regulator, $Cl^-/HCO3^-$ exchanger (SLC26A6), sodium-hydrogen exchanger-1, CA isoenzymes II and XII [64, 65], and possibly epithelial Na^+ channel [66], also regulates uterine lumen pH. Based on the reduced D4.5 implantation rate and retained zona pellucida of D4.5 blastocysts from *Atp6v0d2*$^{-/-}$ females without implantation sites in the first mating, *Atp6v0d2*-deficiency might initially affect the uterine lumen pH, thus timely blastocyst development and hatching from zona pellucida for embryo implantation in some *Atp6v0d2*$^{-/-}$ mice, which subsequently adapted to *Atp6v0d2*-deficiency and had normal fertility.

It was noticed that *Atp6v0d2* mRNA in the D4.5 LE at the implantation chamber was lower than its level in the D4.5 LE at interimplantation site, whereas D4.5 LE acidification at implantation site was comparable, if not stronger, than that at interimplantation site; and that upregulation of *Atp6v0d2* mRNA upon embryo implantation was mainly detected in the LE but not in the GE, yet GE and LE had comparable acidification upon embryo implantation. These

observations suggest that Atp6v0d2 subunit may not play an important role in LE acidification at the implantation site or in GE acidification, and different mechanisms may be involved in regulating acidification of LE at the implantation site and the interimplantation site, and acidification of GE upon embryo implantation.

V-ATPase activity is regulated at multiple levels, such as transcriptional and/or translational regulation of subunits, domain assembly, alternative subunits (e.g., *Atp6v0d1* also encodes a d subunit), and targeting of subunits to specific membranes [11–13, 67]. No significant compensatory transcriptional regulation of V0 subunits (especially *Atp6v0d1*) and counter ion channels in D4.5 *Atp6v0d2*$^{-/-}$ LE coupled with no obviously impaired fertility in *Atp6v0d2*$^{-/-}$ females suggests nonessential role of Atp6v0d2 subunit in embryo implantation, and/or compensatory regulations of other V-ATPase subunits and/or counter ions at levels other than transcription, such as translation, domain assembly, etc. [11–13, 67]. The data from *Atp6v0d2*$^{-/-}$ females cannot exclude potential function of V-ATPase as a whole unit in embryo implantation.

To determine the potential function of V-ATPase on embryo implantation, we took advantage of a pharmacological approach using the specific V-ATPase inhibitor bafilomycin A1 [68] coupled with uterine fat pad injection [39–45]. We noticed that the lower dose of bafilomycin A1 (0.5 μg/kg) via uterine fat pad injection caused an adverse effect mainly on the injected side, while the higher dose (2.5 μg/kg) had an adverse effect on both uterine horns, suggesting that sufficient levels of the drug might be transported to the uninjected uterine horn through the local uterine blood supply. The data from uterine fat pad injection of bafilomycin A1 demonstrated a critical role of V-ATPase for uterine function in embryo implantation. However, with this approach, the roles of V-ATPase in different uterine compartments (e.g., uterine epithelium, stroma, myometrium) on embryo implantation could not be differentiated.

This study demonstrated the novel phenomenon of uterine epithelial acidification upon embryo implantation and the involvement of V-ATPase in regulating uterine epithelial acidification and uterine preparation for embryo implantation. V-ATPase plays an essential role in regulating lysosomal acidification [23], which affects the functions of lysosomes in intracellular metabolism and nutrient homeostasis in many cell types [69]. The molecular mechanisms for lysosomal acidification in uterine epithelium as well as the functions of uterine epithelial acidification in the initial uterine-embryo communications and uterine epithelial-stromal paracrine communications remain to be investigated.

Acknowledgments

Authors thank the Office of the Vice President for Research, Interdisciplinary Toxicology Program, and Department of Physiology and Pharmacology at University of Georgia. This work was supported by the National Institutes of Health grants to XY: NIH R15HD066301 and NIH R01HD065939 (co-funded by Office of Research on Women's Health (ORWH) and Eunice Kennedy Shriver National Institute of Child Health and Human Development (NICHD).

Conflict of interest statement: The authors declare that there are no conflicts of interest.

References

1. Jones CJ, Aplin JD. Glycosylation at the fetomaternal interface: does the glycocode play a critical role in implantation? *Glycoconj J* 2009; **26**:359–366.
2. Schlafke S, Enders AC. Cellular basis of interaction between trophoblast and uterus at implantation. *Biol Reprod* 1975; **12**:41–65.
3. Yoshinaga K. A sequence of events in the uterus prior to implantation in the mouse. *J Assist Reprod Genet* 2013; **30**:1017–1022.
4. Xiao S, Diao H, Zhao F, Li R, He N, Ye X. Differential gene expression profiling of mouse uterine luminal epithelium during periimplantation. *Reprod Sci* 2014; **21**:351–362.
5. Denker HW. Implantation: a cell biological paradox. *J Exp Zool* 1993; **266**:541–558.
6. Spencer TE. Biological roles of uterine glands in pregnancy. *Semin Reprod Med* 2014; **32**:346–357.
7. Murphy CR. Uterine receptivity and the plasma membrane transformation. *Cell Res* 2004; **14**:259–267.
8. Xiao S, Diao H, Zhao F, Li R, He N, Ye X. Differential gene expression profiling of mouse uterine luminal epithelium during periimplantation. *Reprod Sci* 2013; **21**:351–362.
9. Lee W. Electron microscopic observations of the rat endometrium during the implantation period, with special reference to its sex steroid hormone regulation (author's transl). *Nihon Naibunpi Gakkai Zasshi* 1975; **51**:938–966.
10. Toei M, Saum R, Forgac M. Regulation and isoform function of the V-ATPases. *Biochemistry* 2010; **49**:4715–4723.
11. Forgac M. Structure and properties of the vacuolar (H+)-ATPases. *J Biol Chem* 1999; **274**:12951–12954.
12. Qi J, Wang Y, Forgac M. The vacuolar (H+)-ATPase: subunit arrangement and in vivo regulation. *J Bioenerg Biomembr* 2007; **39**: 423–426.
13. Smith AN, Lovering RC, Futai M, Takeda J, Brown D, Karet FE. Revised nomenclature for mammalian vacuolar-type H+ -ATPase subunit genes. *Mol Cell* 2003; **12**:801–803.
14. Sun-Wada GH, Wada Y, Futai M. Diverse and essential roles of mammalian vacuolar-type proton pump ATPase: toward the physiological understanding of inside acidic compartments. *Biochim Biophys Acta* 2004; **1658**:106–114.
15. Toyomura T, Murata Y, Yamamoto A, Oka T, Sun-Wada GH, Wada Y, Futai M. From lysosomes to the plasma membrane: localization of vacuolar-type H+-ATPase with the a3 isoform during osteoclast differentiation. *J Biol Chem* 2003; **278**:22023–22030.
16. Da Silva N, Shum WW, Breton S. Regulation of vacuolar proton pumping ATPase-dependent luminal acidification in the epididymis. *Asian J Androl* 2007; **9**:476–482.
17. Herak-Kramberger CM, Sabolic I, Blanusa M, Smith PJ, Brown D, Breton S. Cadmium inhibits vacuolar H(+)ATPase-mediated acidification in the rat epididymis. *Biol Reprod* 2000; **63**:599–606.
18. Pietrement C, Sun-Wada GH, Silva ND, McKee M, Marshansky V, Brown D, Futai M, Breton S. Distinct expression patterns of different subunit isoforms of the V-ATPase in the rat epididymis. *Biol Reprod* 2006; **74**:185–194.
19. Blomqvist SR, Vidarsson H, Soder O, Enerback S. Epididymal expression of the forkhead transcription factor Foxi1 is required for male fertility. *EMBO J* 2006; **25**:4131–4141.
20. Yeung CH, Breton S, Setiawan I, Xu Y, Lang F, Cooper TG. Increased luminal pH in the epididymis of infertile c-ros knockout mice and the expression of sodium-hydrogen exchangers and vacuolar proton pump H+-ATPase. *Mol Reprod Dev* 2004; **68**:159–168.
21. Skinner MA, MacLaren LA, Wildeman AG. Stage-dependent redistribution of the V-ATPase during bovine implantation. *J Histochem Cytochem* 1999; **47**:1247–1254.
22. Kirk AT, Murphy CR. Increase in lysosomal numbers and activity in the rat uterine luminal and glandular epithelium during early pregnancy: a histochemical study. *Acta Anat (Basel)* 1991; **141**:63–69.
23. Ishida Y, Nayak S, Mindell JA, Grabe M. A model of lysosomal pH regulation. *J Gen Physiol* 2013; **141**:705–720.
24. Lee SH, Rho J, Jeong D, Sul JY, Kim T, Kim N, Kang JS, Miyamoto T, Suda T, Lee SK, Pignolo RJ, Koczon-Jaremko B, et al. v-ATPase V0 subunit d2-deficient mice exhibit impaired osteoclast fusion and increased bone formation. *Nat Med* 2006; **12**:1403–1409.

25. Diao H, Li R, El Zowalaty AE, Xiao S, Zhao F, Dudley EA, Ye X. Deletion of lysophosphatidic acid receptor 3 (Lpar3) disrupts fine local balance of progesterone and estrogen signaling in mouse uterus during implantation. *Biol Reprod* 2015; **93**:123.
26. Diao H, Aplin JD, Xiao S, Chun J, Li Z, Chen S, Ye X. Altered spatiotemporal expression of collagen types I, III, IV, and VI in Lpar3-deficient peri-implantation mouse uterus. *Biol Reprod* 2011; **84**:255–265.
27. Ye X, Herr DR, Diao H, Rivera R, Chun J. Unique uterine localization and regulation may differentiate LPA3 from other lysophospholipid receptors for its role in embryo implantation. *Fertil Steril* 2011; **95**:2107–2113.
28. Ye X, Hama K, Contos JJ, Anliker B, Inoue A, Skinner MK, Suzuki H, Amano T, Kennedy G, Arai H, Aoki J, Chun J. LPA3-mediated lysophosphatidic acid signalling in embryo implantation and spacing. *Nature* 2005; **435**:104–108.
29. Xiao S, Li R, Diao H, Zhao F, Ye X. Progesterone receptor-mediated regulation of n-acetylneuraminate pyruvate lyase (NPL) in mouse uterine luminal epithelium and nonessential role of NPL in uterine function. *PLoS One* 2013; **8**:e65607.
30. Diao H, Xiao S, Li R, Zhao F, Ye X. Distinct spatiotemporal expression of serine proteases prss23 and prss35 in periimplantation mouse uterus and dispensable function of prss35 in fertility. *PLoS One* 2013; **8**:e56757.
31. Diao H, Xiao S, Zhao F, Ye X. Uterine luminal epithelium-specific proline-rich acidic protein 1 (PRAP1) as a marker for successful embryo implantation. *Fertil Steril* 2010; **94**:2808–2811.
32. Ishiguro K, Ando T, Watanabe O, Goto H. Novel application of low pH-dependent fluorescent dyes to examine colitis. *BMC Gastroenterol* 2010; **10**:4.
33. Perzov N, Padler-Karavani V, Nelson H, Nelson N. Characterization of yeast V-ATPase mutants lacking Vph1p or Stv1p and the effect on endocytosis. *J Exp Biol* 2002; **205**:1209–1219.
34. Bigler L, Spirli C, Fiorotto R, Pettenazzo A, Duner E, Baritussio A, Follath F, Ha HR. Synthesis and cytotoxicity properties of amiodarone analogues. *Eur J Med Chem* 2007; **42**:861–867.
35. Teichgraber V, Ulrich M, Endlich N, Riethmuller J, Wilker B, De Oliveira-Munding CC, van Heeckeren AM, Barr ML, von Kurthy G, Schmid KW, Weller M, Tummler B et al. Ceramide accumulation mediates inflammation, cell death and infection susceptibility in cystic fibrosis. *Nat Med* 2008; **14**:382–391.
36. Byers SL, Wiles MV, Dunn SL, Taft RA. Mouse estrous cycle identification tool and images. *PLoS One* 2012; **7**:e35538.
37. Li R, Diao H, Zhao F, Xiao S, El Zowalaty AE, Dudley EA, Mattson MP, Ye X. Olfactomedin 1 deficiency leads to defective olfaction and impaired female fertility. *Endocrinology* 2015; **156**:3344–3357.
38. Li R, Zhao F, Diao H, Xiao S, Ye X. Postweaning dietary genistein exposure advances puberty without significantly affecting early pregnancy in C57BL/6J female mice. *Reprod Toxicol* 2014; **44**:85–92.
39. Diao H, Xiao S, Howerth EW, Zhao F, Li R, Ard MB, Ye X. Broad gap junction blocker carbenoxolone disrupts uterine preparation for embryo implantation in mice. *Biol Reprod* 2013; **89**:31.
40. Yoshinaga K. Effect of local application of ovarian hormones on the delay in implantation in lactating rats. *J Reprod Fertil* 1961; **2**:35–41.
41. Yoshinaga K. On the delayed implantation in the lactating pregnant rat. III. The local action of progesterone. *Jpn J Anim Reprod* 1961; **6**:152–154.
42. Yoshinaga K. On the delayed implantation in the lactating pregnant rat. IV. The local action of estrogen. *Jpn J Anim Reprod* 1961; **6**:155–158.
43. Yoshinaga K, Pincus G. Local effect of estrogen on cholesterol synthesis in the uterus of ovariectomized rats. *Steroids* 1963; **1**:656–663.
44. Ferrando G, Nalbandov AV. Relative importance of histamine and estrogen on implantation in rats. *Endocrinology* 1968; **83**:933–937.
45. Psychoyos A. New remarks on the determinism of ovum implantation. *C R Hebd Seances Acad Sci* 1962; **254**:4360–4362.
46. Drose S, Altendorf K. Bafilomycins and concanamycins as inhibitors of V-ATPases and P-ATPases. *J Exp Biol* 1997; **200**:1–8.
47. Lim H, Paria BC, Das SK, Dinchuk JE, Langenbach R, Trzaskos JM, Dey SK. Multiple female reproductive failures in cyclooxygenase 2-deficient mice. *Cell* 1997; **91**:197–208.
48. Liang XH, Zhao ZA, Deng WB, Tian Z, Lei W, Xu X, Zhang XH, Su RW, Yang ZM. Estrogen regulates amiloride-binding protein 1 through CCAAT/enhancer-binding protein-beta in mouse uterus during embryo implantation and decidualization. *Endocrinology* 2010; **151**:5007–5016.
49. Diao H, Paria BC, Xiao S, Ye X. Temporal expression pattern of progesterone receptor in the uterine luminal epithelium suggests its requirement during early events of implantation. *Fertil Steril* 2011; **95**:2087–2093.
50. Mindell JA. Lysosomal acidification mechanisms. *Annu Rev Physiol* 2012; **74**:69–86.
51. Zhao F, Li R, Xiao S, Diao H, Viveiros MM, Song X, Ye X. Postweaning exposure to dietary zearalenone, a mycotoxin, promotes premature onset of puberty and disrupts early pregnancy events in female mice. *Toxicol Sci* 2013; **132**:431–442.
52. Xiao S, Diao H, Smith MA, Song X, Ye X. Preimplantation exposure to bisphenol A (BPA) affects embryo transport, preimplantation embryo development, and uterine receptivity in mice. *Reprod Toxicol* 2011; **32**:434–441.
53. Sengupta J, Roy SK, Manchanda SK. Hormonal control of implantation: a possible role of lysosomal function in the embryo-uterus interaction. *J Steroid Biochem* 1979; **11**:729–744.
54. Leiser R, Wille KH. Cytochemical establishment of acid phosphatase in the bovine endometrium and trophoblast during implantation. *Anat Embryol (Berl)* 1975; **148**:159–173.
55. Burney RO, Talbi S, Hamilton AE, Vo KC, Nyegaard M, Nezhat CR, Lessey BA, Giudice LC. Gene expression analysis of endometrium reveals progesterone resistance and candidate susceptibility genes in women with endometriosis. *Endocrinology* 2007; **148**:3814–3826.
56. Casey JR, Grinstein S, Orlowski J. Sensors and regulators of intracellular pH. *Nat Rev Mol Cell Biol* 2010; **11**:50–61.
57. Xu H, Ren D. Lysosomal physiology. *Annu Rev Physiol* 2015; **77**:57–80.
58. Oka T, Murata Y, Namba M, Yoshimizu T, Toyomura T, Yamamoto A, Sun-Wada GH, Hamasaki N, Wada Y, Futai M. a4, a unique kidney-specific isoform of mouse vacuolar H+-ATPase subunit a. *J Biol Chem* 2001; **276**:40050–40054.
59. Wagner CA, Finberg KE, Breton S, Marshansky V, Brown D, Geibel JP. Renal vacuolar H+-ATPase. *Physiol Rev* 2004; **84**:1263–1314.
60. Peng SB, Li X, Crider BP, Zhou Z, Andersen P, Tsai SJ, Xie XS, Stone DK. Identification and reconstitution of an isoform of the 116-kDa subunit of the vacuolar proton translocating ATPase. *J Biol Chem* 1999; **274**:2549–2555.
61. Smith AN, Borthwick KJ, Karet FE. Molecular cloning and characterization of novel tissue-specific isoforms of the human vacuolar H(+)-ATPase C, G and d subunits, and their evaluation in autosomal recessive distal renal tubular acidosis. *Gene* 2002; **297**:169–177.
62. Karet FE, Finberg KE, Nelson RD, Nayir A, Mocan H, Sanjad SA, Rodriguez-Soriano J, Santos F, Cremers CW, Di Pietro A, Hoffbrand BI, Winiarski J et al. Mutations in the gene encoding B1 subunit of H+-ATPase cause renal tubular acidosis with sensorineural deafness. *Nat Genet* 1999; **21**:84–90.
63. Li X, Chai Y, Tao Z, Li L, Huang Z, Li Y, Wu H, Yang T. Novel mutations in ATP6V0A4 are associated with atypical progressive sensorineural hearing loss in a Chinese patient with distal renal tubular acidosis. *Int J Pediatr Otorhinolaryngol* 2012; **76**:152–154.
64. Karim K, Giribabu N, Muniandy S, Salleh N. Vacuolar-ATPase (V-ATPase) mediates progesterone-induced uterine fluid acidification in rats. *J Membr Biol* 2016; **249**:65–76.
65. Gholami K, Muniandy S, Salleh N. *In-vivo* functional study on the involvement of CFTR, SLC26A6, NHE-1 and CA isoenzymes II and XII in uterine fluid pH, volume and electrolyte regulation in rats under different sex-steroid influence. *Int J Med Sci* 2013; **10**:1121–1134.
66. Ruan YC, Guo JH, Liu X, Zhang R, Tsang LL, Dong JD, Chen H, Yu MK, Jiang X, Zhang XH, Fok KL, Chung YW et al. Activation of the epithelial Na+ channel triggers prostaglandin E(2) release and production required for embryo implantation. *Nat Med* 2012; **18**:1112–1117.

67. O'Callaghan KM, Ayllon V, O'Keeffe J, Wang Y, Cox OT, Loughran G, Forgac M, O'Connor R. Heme-binding protein HRG-1 is induced by insulin-like growth factor I and associates with the vacuolar H+-ATPase to control endosomal pH and receptor trafficking. *J Biol Chem* 2010; **285**:381–391.
68. Yoshimori T, Yamamoto A, Moriyama Y, Futai M, Tashiro Y. Bafilomycin A1, a specific inhibitor of vacuolar-type H(+)-ATPase, inhibits acidification and protein degradation in lysosomes of cultured cells. *J Biol Chem* 1991; **266**:17707–17712.
69. Colacurcio DJ, Nixon RA. Disorders of lysosomal acidification-The emerging role of v-ATPase in aging and neurodegenerative disease. *Ageing Res Rev* 2016; **32**:75–88.